BEAM TRANSPORT STUDIES ON THE PROTON BEAM LINE IN THE INJECTOR COMPLEX OF LAMPF*

by

R. R. Stevens, Jr., B. Goplen, J. Stovall

University of California
Los Alamos Scientific Laboratory
Los Alamos, New Mexico

ABSTRACT

As a result of beam measurements made at the exit of the accelerating column in the high-intensity proton injector, additional quadrupole lenses have been incorporated in the proton beam transport line. The design for the new transport system and the beam measurements subsequently carried out with this new design are presented and the improvement in operation is discussed. Electron neutralization effects have been observed and must be accounted for in the design and operation of this beam line.

I. INTRODUCTION

The initial design for the high intensity proton beam line was based on theoretical considerations of the expected performance of the high-intensity proton injector. The initial design calculations assumed an input beam to the transport system having a beam radius of 0.7 cm and an envelope divergence of ~ 7 mrad. Beam envelope calculations, assuming a Kapchinski-Vladmirski (K-V) phase-space distribution, were carried out using this input beam. Initial experience in the operation of this beam line indicated that beam loss was occuring at the prebuncher for beam currents greater than 20 mA. Beam dynamics studies based on observed emittance measurements implied that the beam size and divergence entering the transport system were larger than initially assumed. Subsequent beam studies carried out at the exit of the accelerating column confirmed this supposition. A new design for the transport system was developed and two additional quadrupole lenses were installed in the beam line which is now able to transport over 30 mA of protons to the linac with minimal loss at the prebuncher. Studies are now in progress to incorporate beam scrapers to eliminate halo beam.

II. INITIAL BEAM TRANSPORT SYSTEM

A layout showing the high-intensity beam transport system is shown in Figs. 1a and 1b together with the original calculated beam profiles in Fig. 2. After initial operation the quadrupole lens strengths in the initial portion of this line were varied to optimize transmission through the prebuncher and the profiles calculated from these new magnet settings are shown in Fig. 3. The beam size at the prebuncher was then smaller than originally designed but no longer at a waist. This mode of operation was satisfactory for transporting proton currents up to 25 mA. However, the prebuncher was still the limiting aperture in the transport line and precluded the transport of larger proton currents which were available from the ion source. The transverse phase-space distributions observed for this beam at three emittance measuring station along the beam line are shown in Fig. 4.

*Work performed under the auspices of the U. S. Atomic Energy Commission.

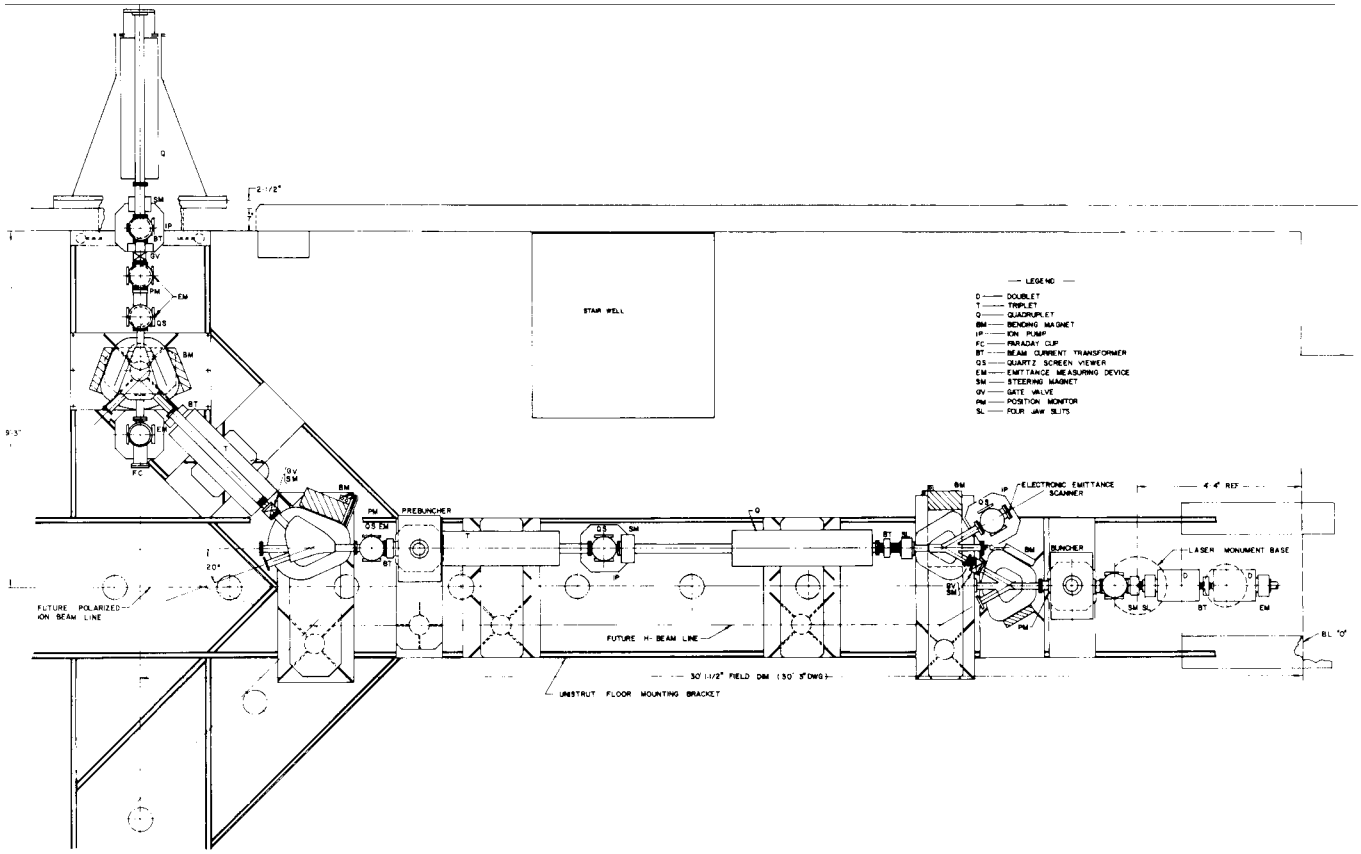

Fig. 1a. Layout of the high-intensity proton-beam line.

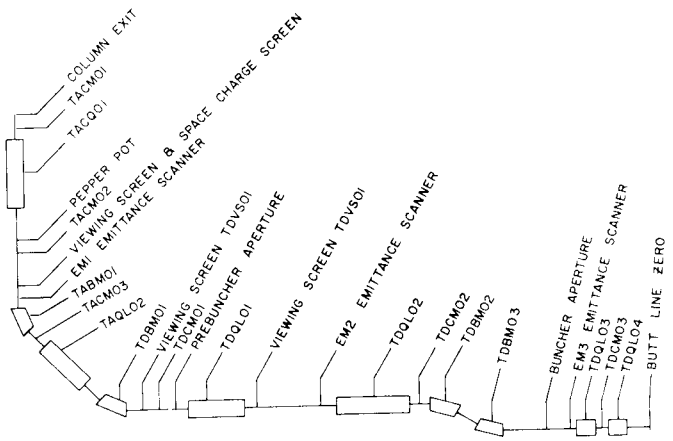

Fig. 1b. Schematic diagram of the high-intensity proton-beam line.

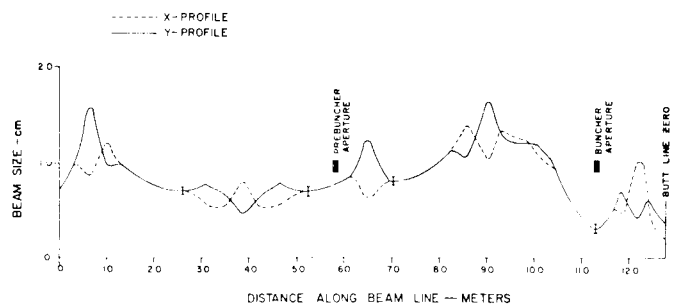

Fig. 2. Beam profiles for original design of the beam transport system.

Beam dynamics calculations were then carried out based on emittance measurements made at the first emittance measuring station. These studies explicitly calculated the space charge interaction between ions and assumed the known admixture of H^+/H_2^+ ions in the beam extracted from the accelerating column. A variant of the PARMILA code (H2PLUS) was used to make these calculations. A parametric search was made to fit the transverse phase space distributions for five different experimental beams at the first emittance measuring station. The beam envelope size and divergence at the exit of the accelerating column and the effective beam current transported were the variables of the search for each beam. The best fit obtained for these five beams was for an input beam to the transport line with 0.8- to 0.9-cm radius and 14-mrad divergence and for an effective space-charge current only 40% of the actual current. The observed and calculated distributions for one of these beams is shown in

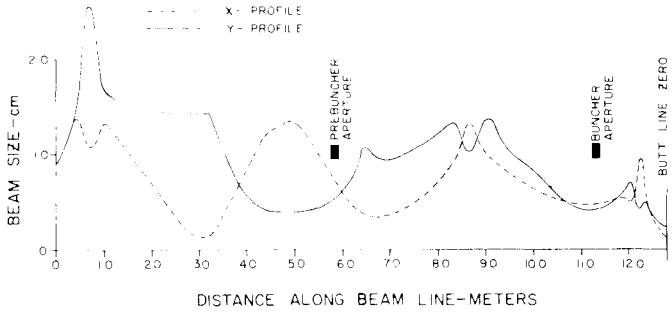

Fig. 3. Calculated beam profiles for the beam initially transported in the high-intensity proton beam line.

Fig. 5. The lower effective current found in this search is believed to reflect space-charge neutralization occuring in the initial part of the transport system where it is known that significant beam loss of H_2^+ ions is occurring.

III. ACCELERATING COLUMN MEASUREMENTS

The difficulty experienced in transporting high current beams through the prebuncher and the results of the beam calculations made on the initial portion of the transport system led to a detailed series of measurements[1] of the beam extracted from the accelerating column. Experiments were done to measure the transverse emittance and the intensity distribution[‡] of this beam for a wide range of ion source parameters. When the accelerating column is operated at the Pierce design current, (that current at which radial acceleration due to the space charge interaction in an ideal uniform density beam is exactly compensated by the focusing forces in the accelerating column), the beam size and divergence observed in these emittance measurements was 1.2-cm radius with 15.1-mrad divergence. Upon extrapolating back 5 in. to the last electrode of the accelerating column and assuming a K-V distribution with 50-mA space charge loading, a beam size of 1.0-cm radius with 14.6-mrad envelope divergence was obtained. These measured values corroborated the beam dynamics calculations made with the H2PLUS code and determined the basic parameters of the beam entering the transport system.

IV. NEW TRANSPORT SYSTEM

Using the values of beam parameters determined from these measurements, new design calculations were carried out to transport the beam extracted from the accelerating column to a small, double waist at the prebuncher aperture. In the course of these calculations, it became apparent that a different configuration of focusing lenses was now needed to meet these constraints. The simplest way of effecting this configuration was to add additional lenses to the existing magnets on the beam line. One lens was added in front of the quadruplet to provide necessary focusing closer to the exit of the column while the second lens was added at the entrance of the first bending magnet to facilitate tuning the beam at the prebuncher entrance. A layout showing the location of these new lenses is shown in Fig. 6.

After the new quadrupole lenses were installed and the beam line put back into operation, emittance measurements and viewing screen observations were taken on the new beam being transported, and the results confirmed the general features of the new design. The phase-space patterns observed at the final emittance measuring station (EM3) for a 28-mA proton beam are shown in Figs. 7 and 8, and the calculated beam profiles and expected phase-space distributions for this beam are shown in Fig. 9. Beam cross sections observed along the beam line are shown in Fig. 10. These observations demonstrated that with these additional lenses proton beams could be transported with the desired double waist at the prebuncher and that higher beam currents could now be transported to the linac.

V. BEAM SCRAPER STUDIES

The beam extracted from the ion source and subsequently transported through the beam line is characterized by a central beam spot and a halo structure. This halo seen in the beam cross sections is a consequence of the tails or satellite crossover structures present in the phase space distribution previously presented. In the operation of LAMPF, it is important to reduce all beam loss in the linac structures and the presence of this halo

[‡]The details of these tests are described in another paper in these proceedings, D. W. Mueller et al., "Operation and Performance of the High-Intensity Proton Injector of LAMPF."

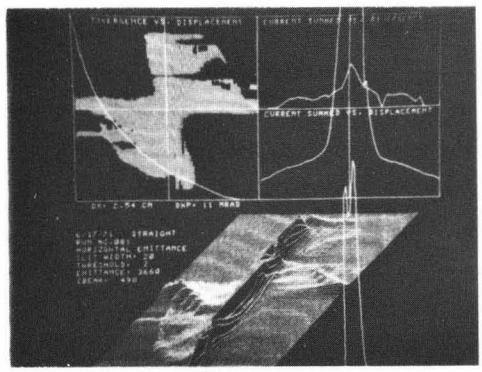

3.7π

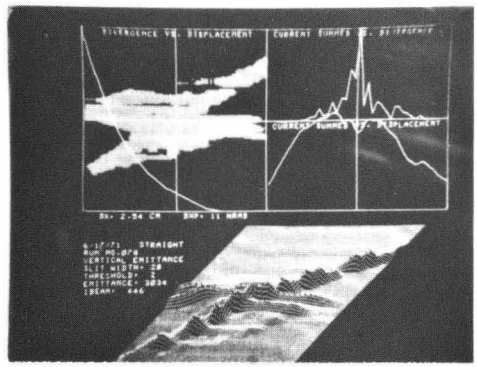

3.0π

EM1

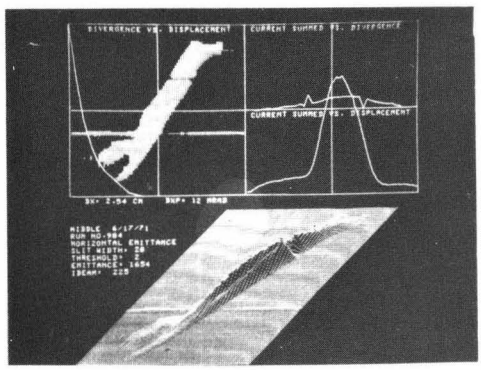

1.0π

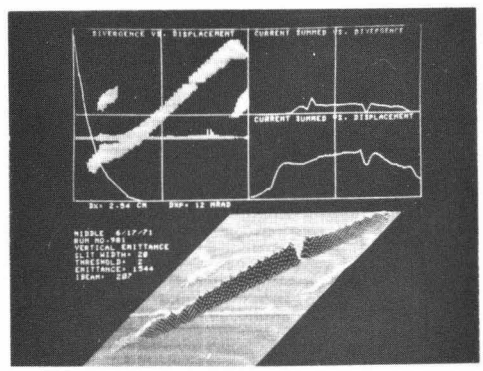

1.5π

EM2

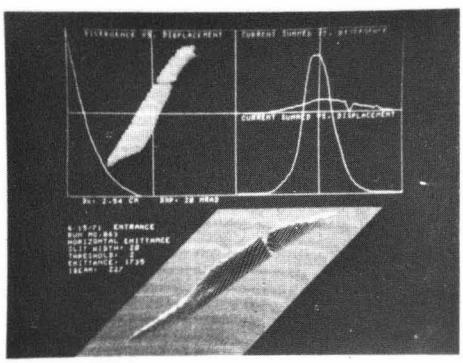

1.7

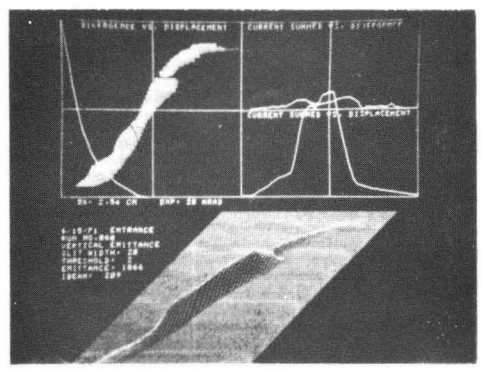

1.9π

EM3

Fig. 4. Observed phase-space distributions for the beam initially transported in the high-intensity proton beam line.

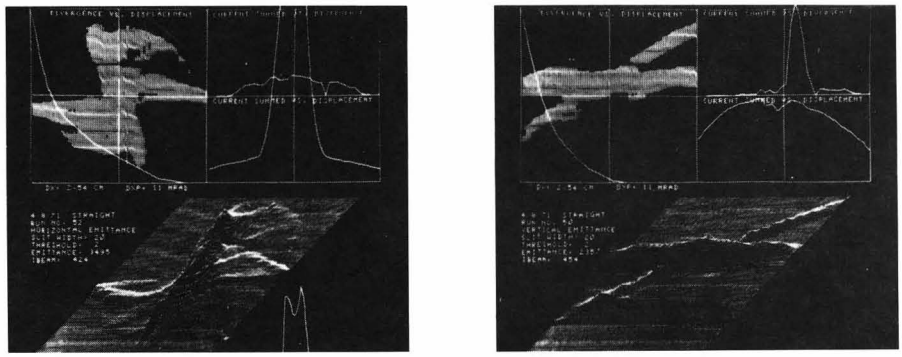

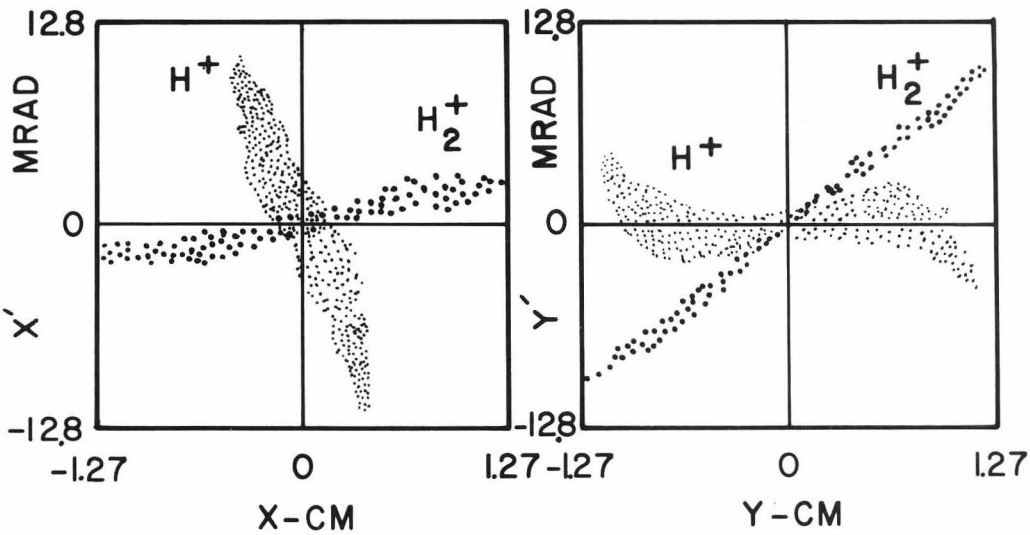

Fig. 5. Observed and calculated phase-space distributions at EM1 for the beam initially transported in the high-intensity proton beam line.

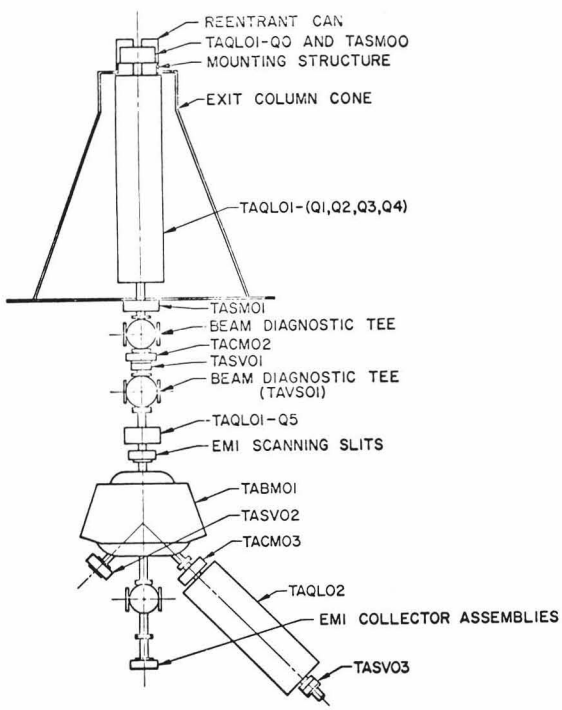

Fig. 6. Layout of the TA beam line showing the location of the two new quadrupole lenses TAQL01-QO and TAQL01-Q5.

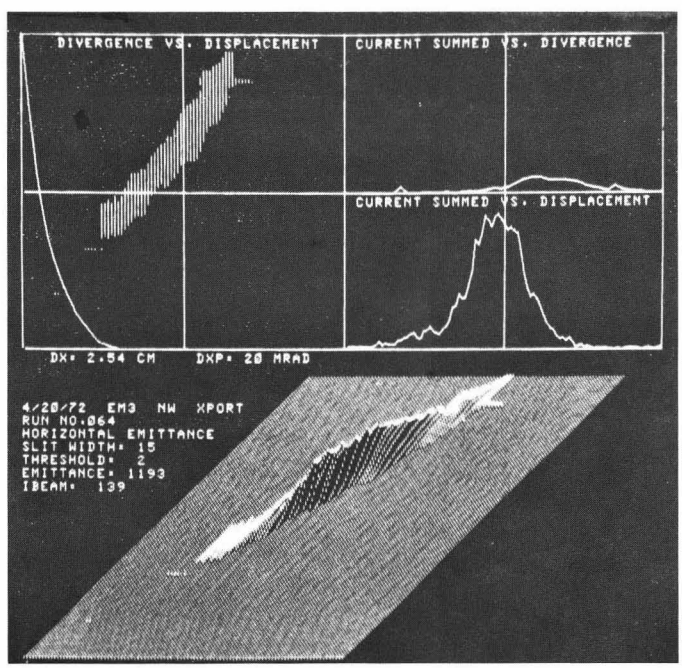

Fig. 7. Horizontal phase-space pattern for a 28-mA proton beam at EM3 after additional quadrupole lenses were installed.

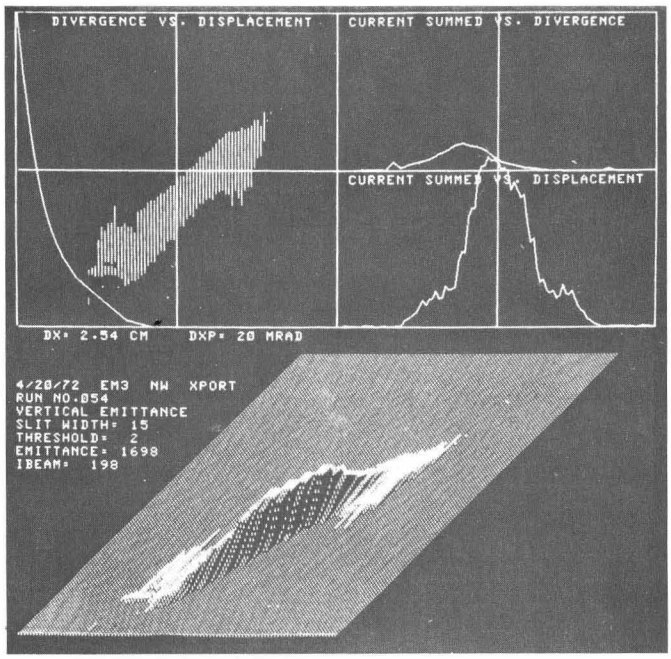

Fig. 8. Vertical phase-space pattern for 28-mA proton beam at EM3 after additional quadrupole lenses were installed.

is believed to be a possible source of beam loss. Studies on scraping these halo structures were therefore initiated, and prototype beam scrapers have been built and installed on the beam line. A photograph of one of these scrapers is shown in Fig. 11. A new beam was empirically determined that minimized

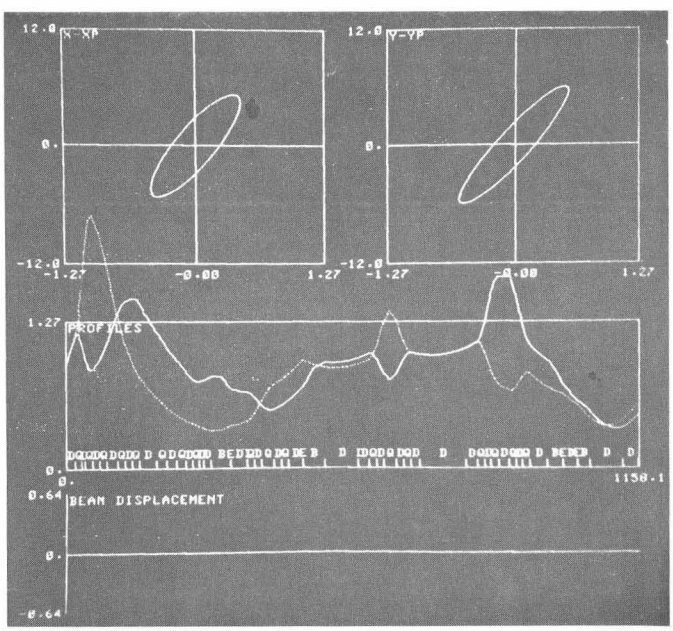

Fig. 9. Calculated beam profiles and phase-space distributions expected at EM3 with the additional quadrupole lenses installed.

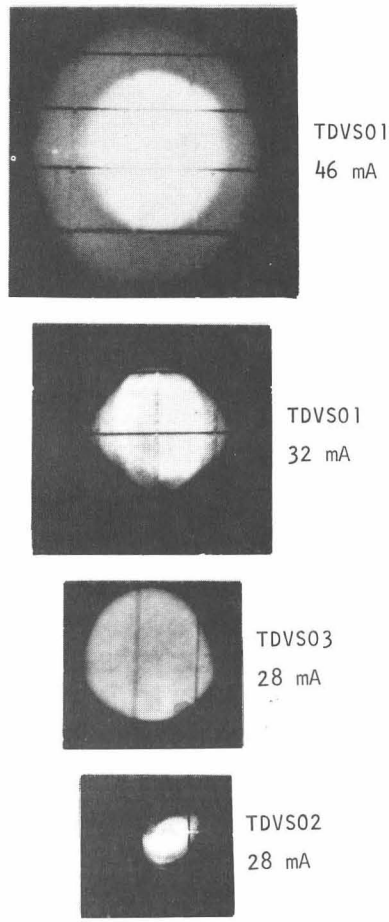

Fig. 10. Beam cross section observed along the beam line with the additional quadrupole lenses installed.

beam size at the bunchers and is now being employed for these beam scraping studies. The phase-space distributions presently obtained at the final emittance measuring station (EM3) with and without these scrapers is shown in Figs. 12-15. The scrapers do

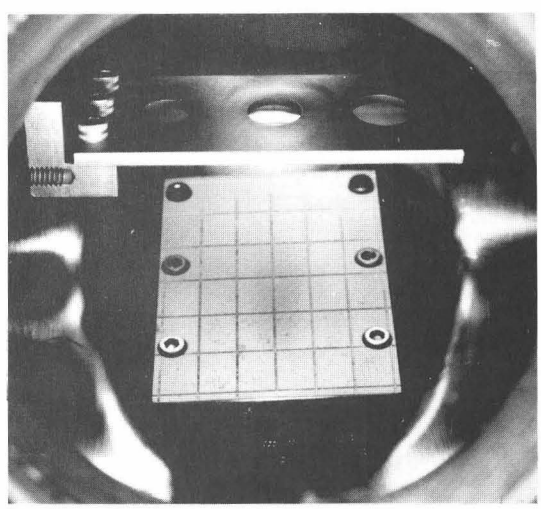

Fig. 11. Prototype beam scraper installed on the high-intensity proton beam line.

remove most of the tails but also result in a rotation of the phase-space distributions. This rotation is the result of the beam scraping that occurs at the first beam scraper located in the initial part of the transport system just in front of the first bending magnet and is presumably as a result of a change in the neutralization of the beam produced when the scraper is inserted into the beam.

The use of beam scrapers has an additional advantage in the tune-up of the transport line. Since this scraper will be designed to permit only the core of the beam to be transported on the design axis, the multiplicity of steering combinations now possible will be reduced. A steering algorithm is being incorporated into a computerized tune-up program that will be based on a stepwise steering to maximize beam through each aperture. Thus these scrapers are expected to facilitate tune-up of this beam line.

REFERENCE

1. R. R. Stevens, Jr., S. D. Palermo, M. A. Paciotti, D. W. Mueller, R. S. Mills, E. A. Meyer, D. K. Kohl and B. Goplen, "Beam Measurements on the High-Intensity Proton Injector of LAMPF," Los Alamos Scientific Laboratory report LA-4961-MS (May 1972).

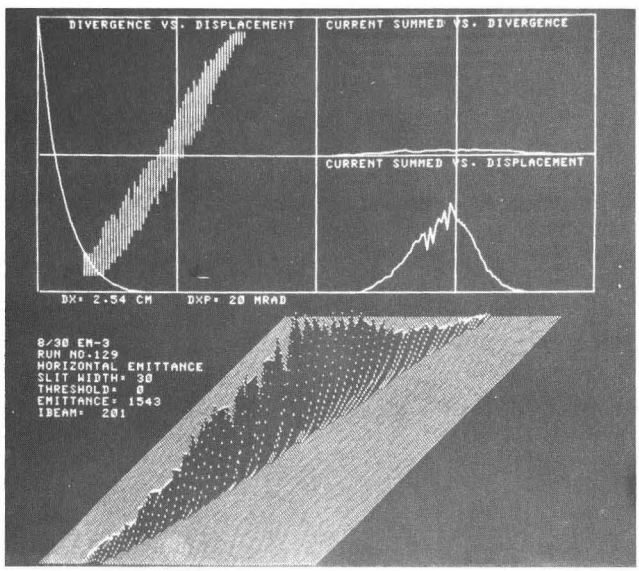

Fig. 12. Horizontal phase-space distribution observed at EM3 without beam scrapers.

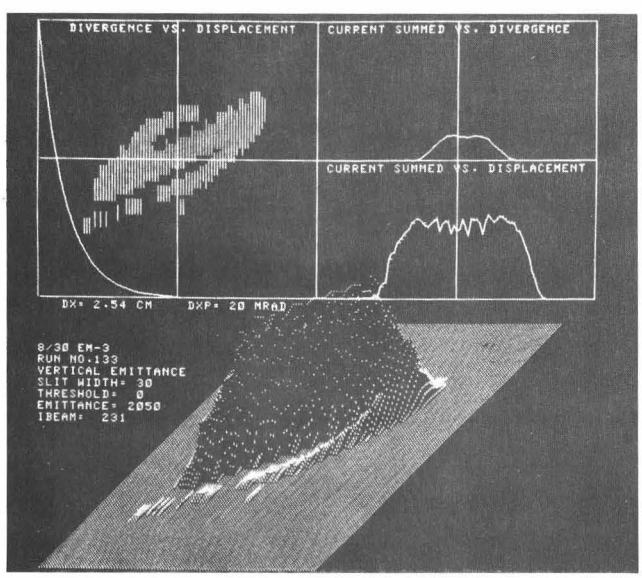

Fig. 13. Vertical phase-space distribution observed at EM3 without beam scrapers

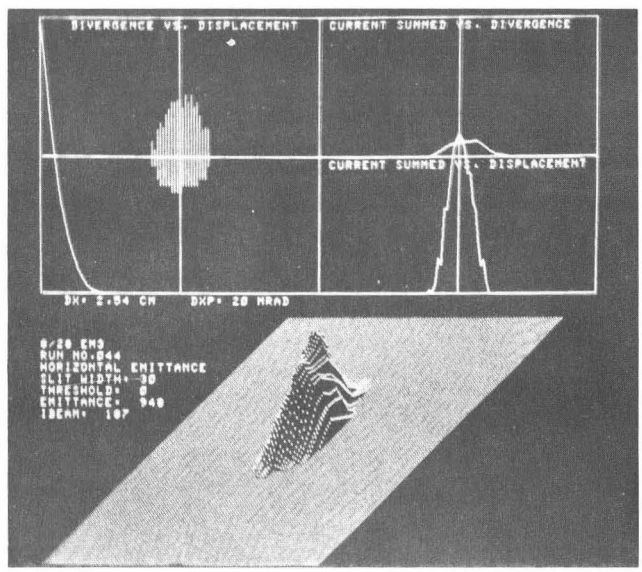

Fig. 14. Horizontal phase-space distribution observed at EM3 with beam scrapers installed on the beam line.

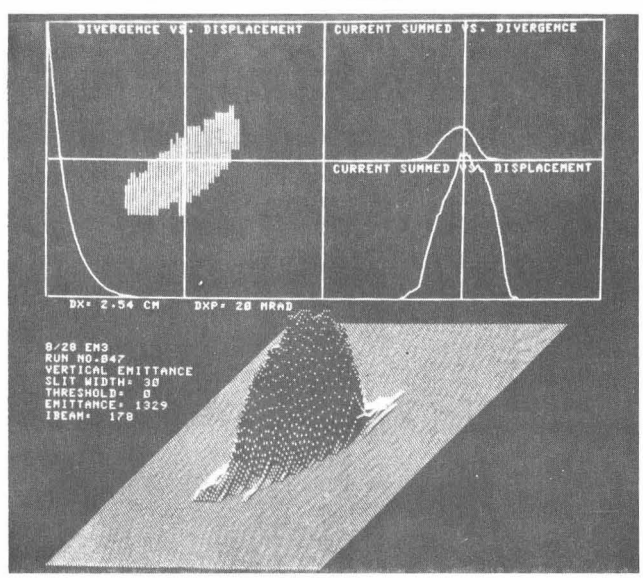

Fig. 15. Vertical phase-space distribution observed at EM3 with beam scrapers installed on the beam line